





RESEARCH ARTICLE | DECEMBER 28 2023

Synthesis and characterization of lithium-doped copper zinc tin sulfide (CZTS) thin films

Md. Maruf Chand ; Shariful Islam ; Mohammad Tanvir Ahmed ; Muhammad Shahriar Bashar ; Farid Ahmed

 Check for updates

AIP Advances 13, 125225 (2023)

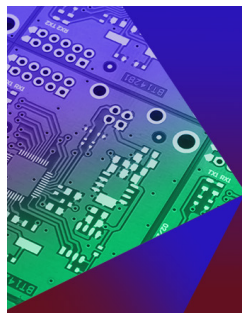
<https://doi.org/10.1063/5.0173862>



View
Online



Export
Citation



APL Electronic Devices

Fostering connections across multiple disciplines
in the broad electronics community

Follow us on  @aplelecdevices

Synthesis and characterization of lithium-doped copper zinc tin sulfide (CZTS) thin films

Cite as: AIP Advances 13, 125225 (2023); doi: 10.1063/5.0173862

Submitted: 25 August 2023 • Accepted: 6 December 2023 •

Published Online: 28 December 2023



View Online



Export Citation



CrossMark

Md. Maruf Chand,^{1,2,a)}  Shariful Islam,²  Mohammad Tanvir Ahmed,³  Muhammad Shahriar Bashar,⁴  and Farid Ahmed²

AFFILIATIONS

¹ Department of CSE, Daffodil International University, Birulia, Dhaka 1216, Bangladesh

² Department of Physics, Jahangirnagar University, Savar, Dhaka 1342, Bangladesh

³ Department of Physics, Jashore University of Science and Technology, Jashore 7408, Bangladesh

⁴ Institute of Fuel and Research Development, Bangladesh Council for Scientific and Industrial Research, Dhanmondi, Dhaka 1205, Bangladesh

^{a)} Author to whom correspondence should be addressed: marufmahmud43@gmail.com

ABSTRACT

The non-toxic nature and remarkable optoelectronic properties of kesterite ($\text{Cu}_2\text{ZnSnS}_4$ and CZTS) make CZTS a potential candidate for solar cell absorber layer material. Since alkali metal doping has shown a performance boost of active layers of solar cells, this work investigates the effects of significant lithium doping on sol-gel-produced CZTS thin films. CZTS- and lithium (Li)-doped CZTS thin films were prepared using the spin coating technique. The variation of structural, morphological, and optical properties of CZTS due to Li-doping has been studied by x-ray diffraction, scanning electron microscopy, and UV-visible spectroscopy techniques. All the synthesized $\text{Li}_x\text{Cu}_{2-x}\text{ZnSnS}_4$ ($x = 0, 0.2, 0.4, 0.6$) films showed fine crystallinity with average crystallite sizes of 4.745, 6.013, 6.255, and 6.404 nm, respectively. The average grain size decreases from 0.336 to 0.310 μm via increasing Li concentration. The inclusion of Li increased the bandgap energy ranges from 1.5 to 1.808 eV. The $\text{Li}_{0.6}\text{Cu}_{1.4}\text{ZnSnS}_4$ thin showed the highest absorption coefficient of $3.505 \times 10^4 \text{ cm}^{-1}$ among all the prepared thin films. A high optical conductivity over 10^{14} s^{-1} was observed for CZTS, which further increased with an increased Li concentration. The synthesized structures showed enhanced characteristics suitable for solar cell application.

© 2023 Author(s). All article content, except where otherwise noted, is licensed under a Creative Commons Attribution (CC BY) license (<http://creativecommons.org/licenses/by/4.0/>). <https://doi.org/10.1063/5.0173862>

I. INTRODUCTION

Solar cells (SCs) are one of the most remarkable inventions of modern technology, which can directly convert solar energy into electricity. At present, the world uses about 4.7×10^{20} Jules of energy per year.¹ The energy crisis is increasing rapidly due to the exponential growth of the world's population. Although, at present, the most common energy demands are met by fossil fuel burning, they are limited, costly, and environmentally unfriendly. Burning fossil fuels causes environmental pollution by generating different types of gases, such as CO_2 , NO_2 , CO, and SO_2 .² The best solution to overcome the energy crisis is to use renewable and eco-friendly energy sources, such as solar, wind, biomass, tidal, and nuclear energy.^{3,4} Among them, solar energy is one of the most promising, environmentally friendly, clean, abundant, and efficient sources.^{5,6}

In recent years, materials, such as CuGaS_2 (CGS), CuInS_2 (CIS), CuInGaSe_2 (CIGS), and CdTe, have demonstrated significant promise as the light-absorbing layer in SCs.^{7,8} Nonetheless, the production of these materials is relatively expensive and may contribute to increased environmental toxicity. As an alternative, $\text{Cu}_2\text{ZnSnS}_4$ (CZTS) has attracted the scientific community due to its non-toxic nature, low fabrication cost, and enhanced optoelectronic performance. Therefore, CZTS has emerged as one of the most encouraging candidates for the absorber layer in thin-film SCs. It possesses a direct bandgap ranging from 1.4 to 1.5 eV and exhibits a substantial absorption coefficient exceeding 10^4 cm^{-1} .^{9,10} According to theoretical observations, the power conversion efficiency (PCE) of CZTS-based solar cells is anticipated to reach ~30%, in accordance with the Shockley-Queisser limit.¹¹ Researchers have developed multiple viable synthetic approaches for CZTS-based SC

fabrication, which fall into two groups. The first is the vacuum approach, including thermal evaporation,¹² DC and RF magnetron sputtering,¹³ pulse laser deposition,¹⁴ electron-beam evaporation,¹⁵ and the second is the non-vacuum approaches, such as spray pyrolysis deposition,¹⁶ electrodeposition,¹⁷ sol-gel sulfurization,¹⁸ and spin coating technique.¹⁹ The non-vacuum spin coating method presents advantages in terms of cost-effectiveness and simplicity, providing a straightforward process for achieving a uniformly grown thin film.

Magorian Friedlmeier *et al.* successfully fabricated thin-film solar cells (SCs) using CZTS as the light absorber, in conjunction with an n-CdS/ZnO window layer in 1997.²⁰ This initial work demonstrated a PCE of up to 2.3%. Subsequent improvements were made, leading to an increased PCE of 5.45% in 2003, and further optimization in 2008 resulted in a PCE of 6.7%, achieved through enhancements to the sulfurization process.^{21,22} Notably, IBM achieved a remarkable PCE of 9.6% for CZTS-based solar cells using a spin coating process with a hydrazine solution.²³ The addition of the MgF₂ antireflection layer improved the PCE up to 10.1%.²⁴ In 2011, Yan *et al.* documented a groundbreaking achievement with a world-record PCE of ~11% for CZTS solar cells.²⁵ However, the pure sulfide CZTS-based thin-film solar cell attained an efficiency of 9%²⁶ in 2016 and 11%²⁵ in 2018. Thus, CZTS is attracting considerable interest for its potential use as an absorbing layer in high-efficiency SCs.

An efficient way to modify the physical properties of semiconductors is by impurity doping. Tong *et al.* explored the influence of Potassium (P) on CZTS films, revealing that P-doping enhances grain sizes while reducing the occurrence of the secondary ZnS phase.²⁷ In a study by Xin *et al.*, lithium (Li) doping in CZTS was found to impact the electric field polarity and decrease the concentration of ZnCu defects.²⁸ Dong *et al.* noted significant effects of Li-doping on adjusting the band-gap and grain boundaries of Cu₂ZnSn(S,Se)₄ (CZTSSe) absorbers, resulting in improved performance of CZTSSe devices.²⁹ Guo *et al.* delved into the optical and electrical properties of Si-doped CZTS films, observing an increase in bandgap and a decrease in carrier concentration.³⁰ The above issues and research motivated us to conduct our study (Fig. 1).

In this research, we have successfully synthesized CZTS thin film via the spin coating method. The structural, morphological, and optical properties of the synthesized film are studied. We have studied the effect of Li dopant concentration on the mentioned properties of the CZTS thin film. The study of different structural properties (e.g., lattice parameter, crystallite size, dislocation density,

strain, etc.) along with different optical properties (e.g., absorbance, absorption coefficient, refractive index, optical conductivity, etc.) are vital for various optoelectronic research works and are the key novelties of this research. To the best of our knowledge, similar studies on Li-doped CZTS have not been previously reported.

II. EXPERIMENTAL SECTION

A. Materials

Copper chloride (CuCl₂ · 2H₂O, 99%, Merck), zinc chloride (ZnCl₂, 98%, Merck), tin chloride (SnCl₂ · 2H₂O, 98%, Merck), thiourea [SC(NH₂)₂, 99%, Merck], and lithium chloride (LiCl, 99%, Merck), monoethanolamine (MEA, 99.5%, Merck), and 2-methoxy ethanol (2-metho, 99%, Merck) were used in this research.

B. Synthesis of pristine and Li-doped CZTS thin film

A 1M solution of CZTS was prepared by dissolving CuCl₂ · 2H₂O, ZnCl₂, SnCl₂ · 2H₂O, and SC(NH₂)₂ in 2-metho maintaining the Cu:Zn:Sn:S molar ratio of 2:1:1:4. A few drops of MEA were added to the mixture during continuous stirring for 30 minutes at 50 °C. Li was doped by adding LiCl in the solution to prepare Li_xCu_{2-x}ZnSnS₄ with x = 0.2, 0.4, and 0.6. Under an ultrasonic bath,

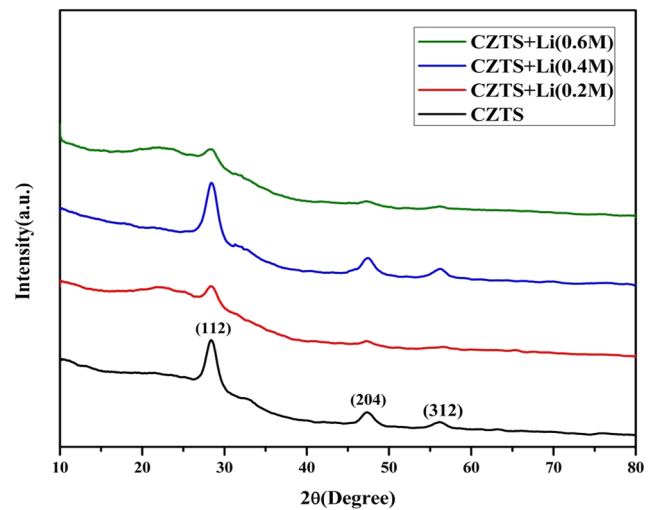


FIG. 2. XRD spectra of the pure and Li-doped CZTS thin film.

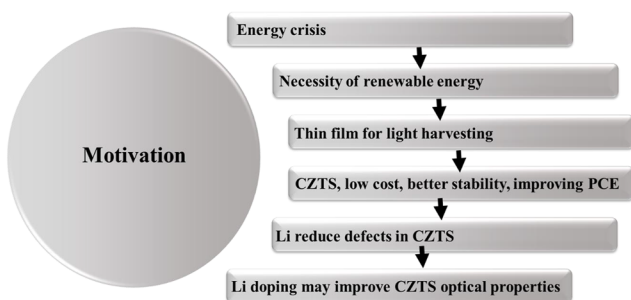


FIG. 1. Schematic diagram of research motivation.

TABLE I. Lattice parameters of CZTS and Li_xCu_{2-x}ZnSnS₄ thin films.

Material	Lattice parameters (Å)			Cell volume (Å ³)
	a	b	c	
Cu ₂ ZnSnS ₄	5.438	5.438	10.845	320.750
Li _x Cu _{2-x} ZnSnS ₄ (x = 0.2M)	5.448	5.448	10.820	321.145
Li _x Cu _{2-x} ZnSnS ₄ (x = 0.4M)	5.455	5.455	10.825	322.128
Li _x Cu _{2-x} ZnSnS ₄ (x = 0.6M)	5.434	5.434	10.833	319.948

the glass substrates were cleaned using distilled water, ethanol, and acetone and dried in the oven. Each composition of $\text{Li}_x\text{Cu}_{2-x}\text{ZnSnS}_4$ solutions was spin-coated on the glass substrate at 1500 rpm for 30 s. The prepared films were dried in an electric oven for 5 min at 50°C . For each sample, the spin-coating and drying procedure was carried out five times to achieve the appropriate thickness and better film coverage. The annealing was carried out at 340°C for 40 min at a heating rate of $9^\circ\text{C}/\text{min}$.

C. Characterization

1. X-ray diffraction (XRD)

The structural properties of the prepared films were obtained using the PW 3040-Xpert x-ray diffractometer with $\text{Cu-K}\alpha$ radiation. The diffraction data were taken in the 2θ angle range of $10\text{--}80^\circ$.

2. Scanning electron microscopy (SEM)

Morphological properties were observed using the ZEISS EVO 18 Scanning Electron Microscope. All images and data were collected at electron high tension (EHT) of 10 kV and a working distance (WD) of 10 mm.

3. UV-visible spectroscopy

The optical properties of the films were observed in the wavelength range from 300 to 800 nm using a double-beam UH4150 UV-VIS spectrophotometer.

III. RESULTS AND DISCUSSION

A. Structural analysis

The x-ray diffraction (XRD) profile of the pristine CZTS thin film displays clear peaks at 2θ values of 28.40° , 47.34° , and 56.15° , representing the (112), (204), and (312) crystallographic planes, respectively (Fig. 2).³¹ The XRD spectra of the CZTS structures do not indicate the presence of any impurities. Although relative changes in peak intensity and peak width are observed due to Li-doping signifying the variation in periodicity and crystallinity, no significant peak shifting is observed.

Table I gives the lattice parameters and cell volumes of the synthesized crystals. All the structures possess a tetragonal phase with a slight deformation from Li doping. It is observed that the cell volume exhibits an initial increase followed by a decrease as the concentration of Li doping increases. Although the cell volume is predicted to increase after Li doping due to the bigger diameter of Li^+ ion compared to Cu^{2+} ion,³² the irregularities in the variation of cell volume can be attributed to the differing thermal expansion coefficients between substrates and deposited films. This variation may generate residual strain in the structures, leading to the deformation of unit cells.³³

The crystallite sizes (D) of the synthesized structures are calculated using the Debye-Scherrer (DS) formula.^{33–35}

Table II shows that the average crystallite size increased with the increase in Li^+ concentration, implying an enhancement in periodicity attributable to the introduction of Li^+ ions. The dislocation

TABLE II. Average crystallite size, dislocation density (ρ), stacking fault (S_F), and lattice strain (ξ) of the prepared crystals.

Samples	Crystallite size (nm)	Dislocation density (ρ) ($1/\text{nm}^2$)	Stacking fault (S_F)	Lattice strain (ξ)
$\text{Cu}_2\text{ZnSnS}_4$	4.745	0.054	0.016	0.032
$\text{Li}_x\text{Cu}_{2-x}\text{ZnSnS}_4$ ($x = 0.2\text{M}$)	6.013	0.031	0.010	0.016
$\text{Li}_x\text{Cu}_{2-x}\text{ZnSnS}_4$ ($x = 0.4\text{M}$)	6.255	0.026	0.0097	0.0155
$\text{Li}_x\text{Cu}_{2-x}\text{ZnSnS}_4$ ($x = 0.6\text{M}$)	6.404	0.025	0.0096	0.0153

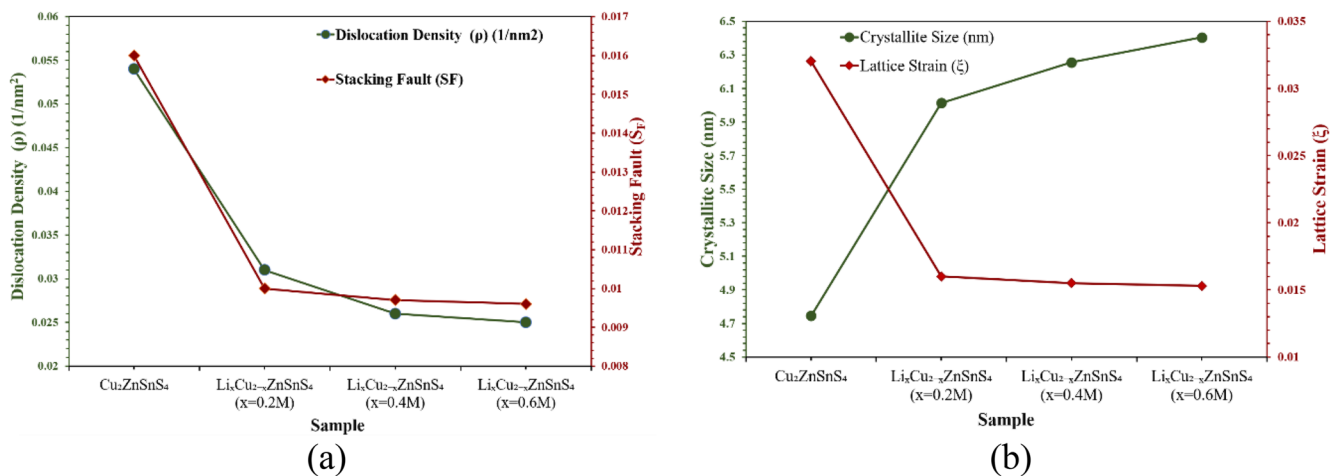


FIG. 3. Variation of (a) dislocation density and stacking fault and (b) crystallite size and lattice strain with increasing Li^+ concentration.

density (ρ), stacking fault (S_F), and lattice strain (ξ) are calculated from the following equations:^{36–38}

$$\rho = \frac{1}{D^2}, \quad (1)$$

$$S_F = \frac{2\pi^2\Gamma}{45(3 \tan \theta)^{\frac{1}{2}}}, \quad (2)$$

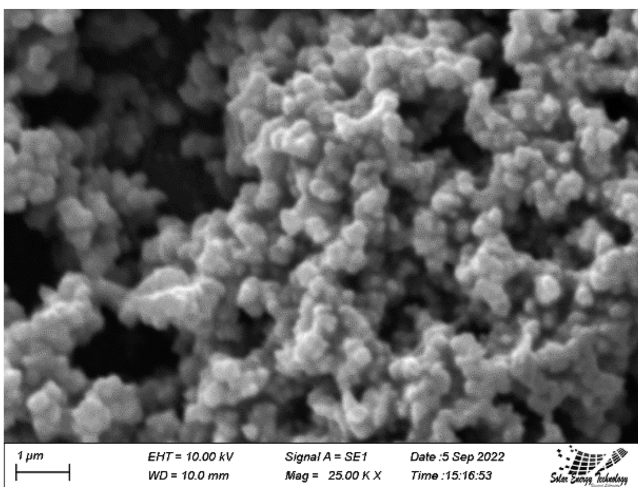
$$\xi = \frac{\Gamma}{4 \tan \theta}. \quad (3)$$

The dislocation density represents the quantity of dislocations per unit length. As the dislocation density adheres to the inverse

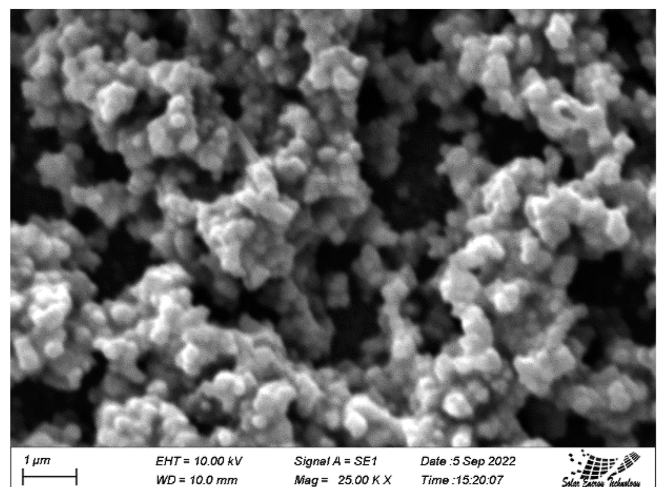
square law with crystallite size, ρ decreases with an increase in Li content in the thin film (Fig. 3). This decrease in the dislocation density is attributed to the improved periodicity, leading to a reduction in stacking faults and lattice strain as Li concentration increases in the thin films. This trend implies a decrease in the imperfections within the periodic structure. The decrease in dislocations and stacking fault suggests a decrease in lattice defects due to Li addition.²⁸ The decrease in dislocations signifies that Li doping caused to decrease in the strength of CZTS material.³⁹

B. Morphological structure of synthesized films

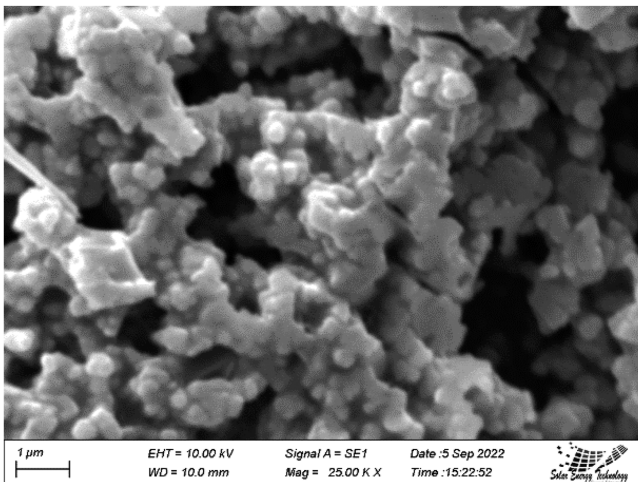
Figure 4 shows the top view of the scanning electron microscopy (SEM) images of the synthesized $\text{Li}_x\text{Cu}_{2-x}\text{ZnSnS}_4$ thin



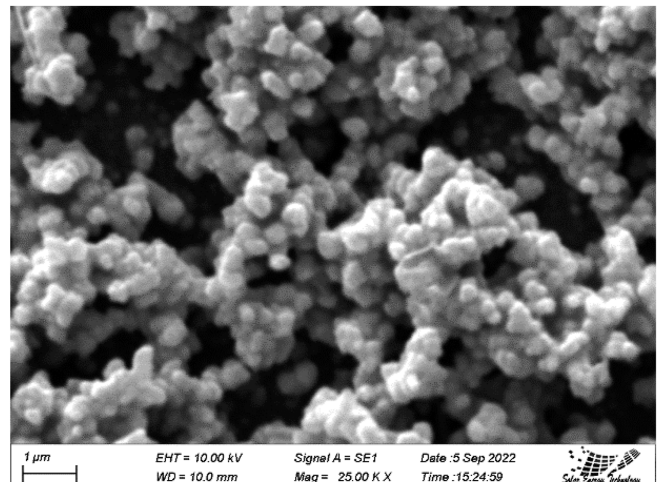
(a)



(b)



(c)



(d)

FIG. 4. SEM images of (a) $\text{Cu}_2\text{ZnSnS}_4$, (b) $\text{Li}_{0.2}\text{Cu}_{1.8}\text{ZnSnS}_4$, (c) $\text{Li}_{0.4}\text{Cu}_{1.6}\text{ZnSnS}_4$, and (d) $\text{Li}_{0.6}\text{Cu}_{1.4}\text{ZnSnS}_4$ thin films.

films, featuring different Li concentrations ($x = 0M, 0.2M, 0.4M, 0.6M$). The SEM analysis reveals no discernible changes in surface morphology corresponding to the varying Li concentration.

All films show tightly packed grains with diameters up to several microns. No significant morphological variation is observed due to Li-doping.²⁸ All the samples exhibited uniform film coverage with spherical grains. The average grain sizes for the CZTS and $\text{Li}_x\text{Cu}_{2-x}\text{ZnSnS}_4$ ($x = 0.2, 0.4, 0.6$) thin films were determined to be 0.336, 0.328, 0.322, and 0.310 μm , respectively.

C. Optical properties

Figure 5 shows the prepared thin films' optical absorbance, reflectance, and transmittance spectrum. All samples show a significant absorption in the visible wavelength region, which decreases with the increase in wavelength. Particularly, the 0.6M Li-doped sample demonstrates the highest absorbance in the visible region. This suggests that the introduction of Li into CZTS enhances its capacity to absorb visible energy. The absorption peak shows a blue shift due to the addition of Li atoms.³²

The reflectance of all samples is consistently high, with slight variations observed within the visible wavelength range. The introduction of Li results in a reduction in the reflectance of the thin films, except for the 0.4M Li-doped thin film. The combination of increased film thickness and uniform film coverage contributes to very low transmittance, which diminishes further with decreasing wavelength across all four samples in the visible region. It is noticed that the transmittance is the minimum for $\text{Li}_x\text{Cu}_{2-x}\text{ZnSnS}_4$ ($x = 0.4M$) thin film.

The absorption coefficient is a vital characteristic of any absorbing layer material for SCs. The prepared thin films' absorption coefficients (α) can be determined using the following equation:⁴⁰

$$\alpha = \frac{2.303A}{t}, \quad (4)$$

where A is the absorbance and t is the thickness. From Fig. 6, it is observed that the absorption coefficient depends on the photon wavelength. In the visible range, all samples have absorption coefficients of more than 10^4 cm^{-1} , making them potential candidates

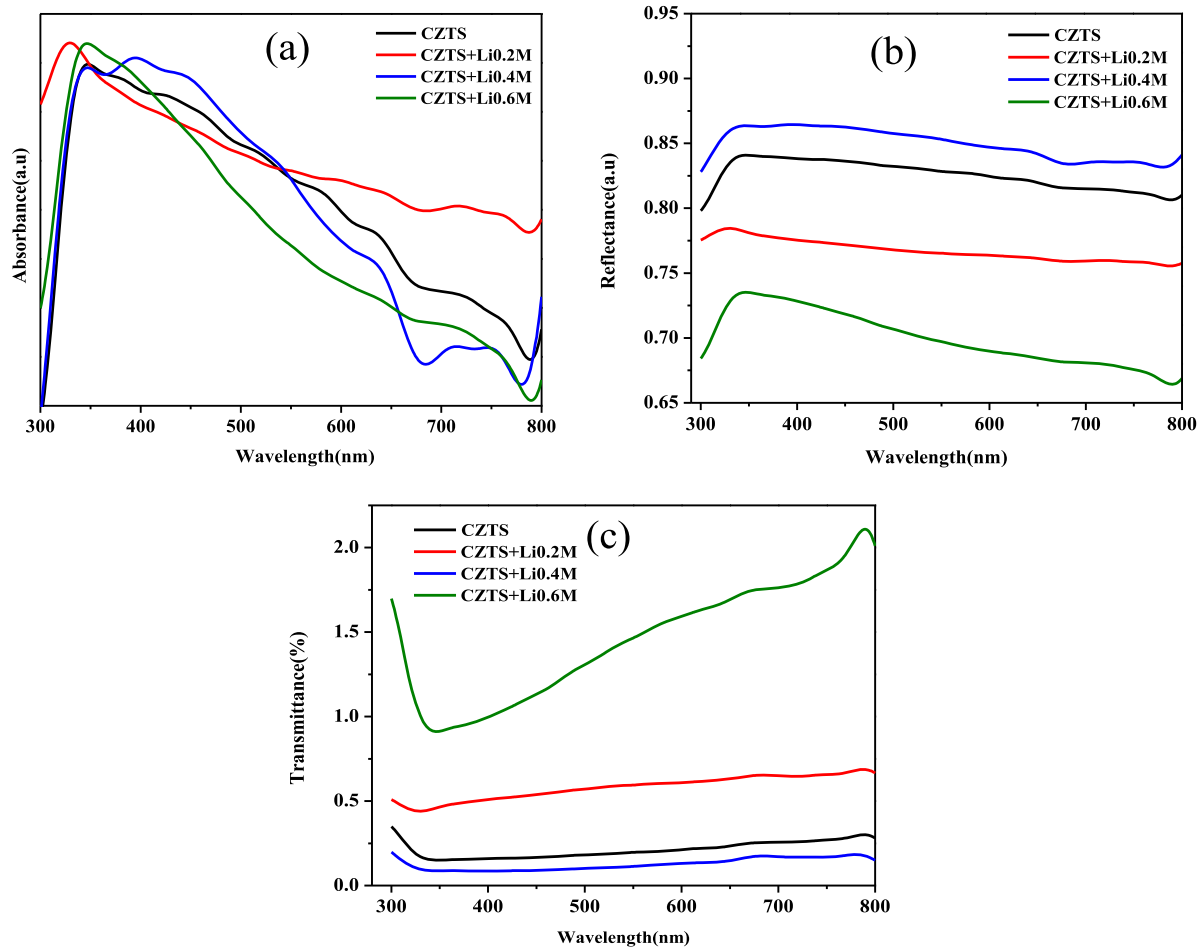


FIG. 5. (a) Absorbance, (b) reflectance, and (c) transmittance spectra of the thin films.

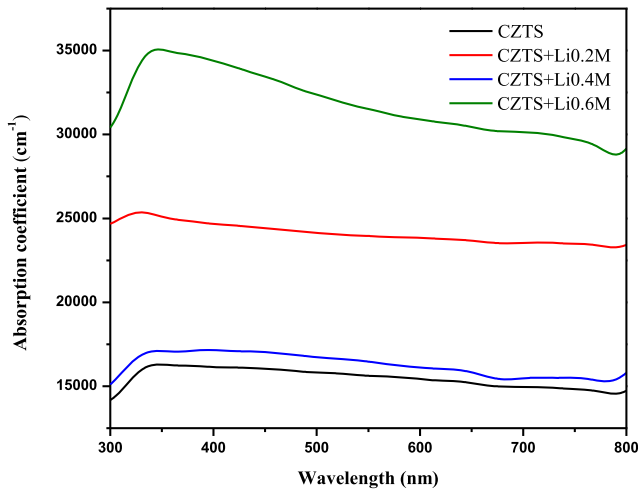


FIG. 6. Absorption coefficients of the thin film.

for SC application. The absorption coefficient for $\text{Li}_x\text{Cu}_{2-x}\text{ZnSnS}_4$ ($x = 0.6$) thin film is higher than the other three samples, and it is $3.505 \times 10^4 \text{ cm}^{-1}$ in the blue wavelength region, which signifies that about 37% of the blue waves are absorbed after traveling $0.285 \mu\text{m}$ thickness. Hence, a few microns thick samples are enough to absorb most of the visible spectrum.

Figure 7 shows the optical bandgap of all the prepared films obtained from the Tauc relation.^{41–43} The bandgap observed for pure CZTS thin film is 1.5 eV.⁴⁴ The Li/Cu ratio has a significant impact on the optoelectronic characteristics of CZTS crystals.³² The optical bandgap of the samples increases from 1.5 to 1.808 eV with increasing Li/Cu ratios (Table III). More precisely, $(\text{Cu}_{0.8}\text{Li}_{0.2})_2\text{ZnSnS}_4$ with a bandgap of 1.7 eV is a very potential choice for top cells in tandem SCs with a Si-based bottom cell.⁴⁵ The bandgap can be a result of structural deformation,³³ as observed in Table I.

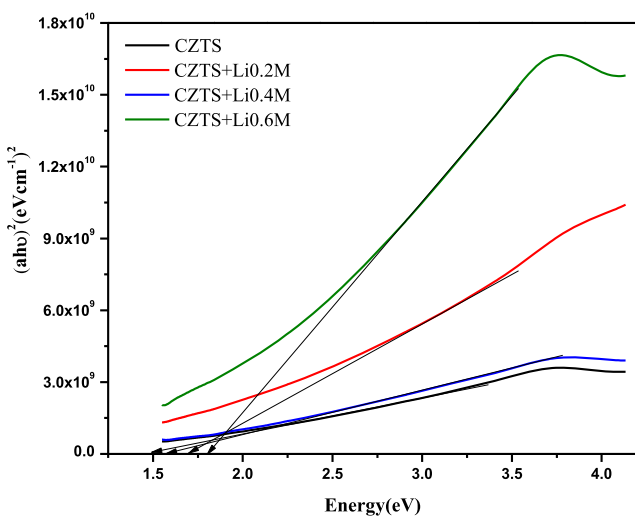


FIG. 7. Tauc plot for the prepared thin films.

TABLE III. Data for optical band gap values of different thin films.

Samples	Film thickness (μm)	Bandgap (E_g) (eV)
$\text{Cu}_2\text{ZnSnS}_4$	3.99	1.5
$\text{Li}_x\text{Cu}_{2-x}\text{ZnSnS}_4$ ($x = 0.2\text{M}$)	2.14	1.704
$\text{Li}_x\text{Cu}_{2-x}\text{ZnSnS}_4$ ($x = 0.4\text{M}$)	4.12	1.504
$\text{Li}_x\text{Cu}_{2-x}\text{ZnSnS}_4$ ($x = 0.6\text{M}$)	1.34	1.808

The extinction coefficient (K) represents the amount of incident energy lost due to absorption or scattering per unit volume of a material. K quantifies the diminution of electromagnetic wave intensity with respect to the wavelength (λ), which can be obtained from the following equation:⁴²

$$K = \frac{\alpha\lambda}{4\pi}. \quad (5)$$

In Fig. 8, the extinction coefficients of the synthesized structure are depicted. The addition of Li content has led to a notable increase in the extinction coefficient of CZTS, particularly in the visible wavelength region. The maximum values of K are observed for $\text{Li}_x\text{Cu}_{2-x}\text{ZnSnS}_4$ ($x = 0.6\text{M}$) thin film.

The refractive index is one of the vital characteristics of a material in optoelectronic research. A lower refractive index suggests transparency for the electromagnetic (EM) spectrum, while a higher refractive index indicates a denser medium affecting the propagation of EM waves. The refractive index of thin films can be determined using the following equation:⁴²

$$\eta = \frac{1+R}{1-R} + \sqrt{\frac{4R}{(1-R)^2} - K^2}, \quad (6)$$

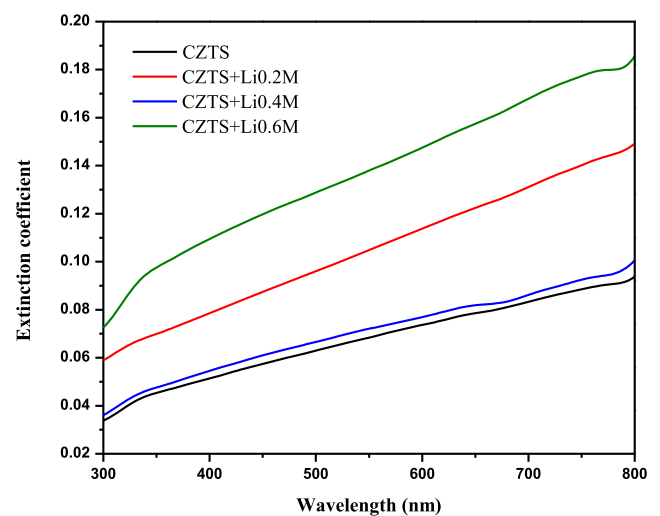


FIG. 8. Extinction coefficient of the prepared thin films.

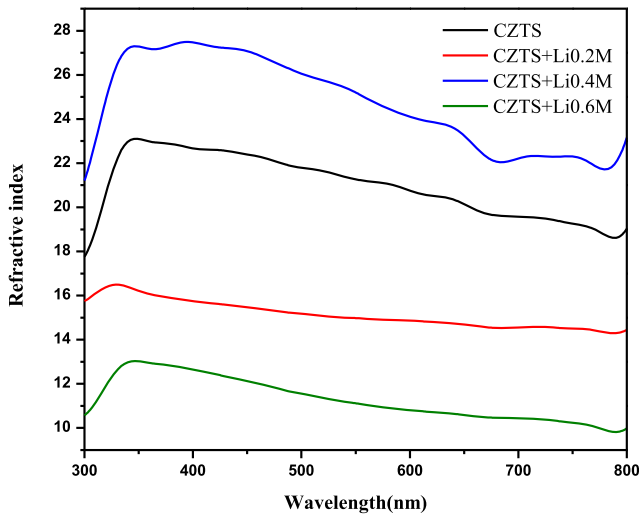


FIG. 9. Refractive index of the thin films.

where K and R are the extinction coefficient and reflectance, respectively.

The CZTS film showed a high refractive index in the visible region, which gradually decreases with increasing wavelength (Fig. 9). Upon the addition of Li-content, there is a subsequent increase in the refractive index. The high refractive index of the CZTS film may be attributed to its high density of the film and this effect could potentially be mitigated by reducing the molar concentration of CZTS.

The complex dielectric constant (ϵ) is a fundamental intrinsic property of materials. The real component of the dielectric constant (ϵ_r) signifies the material's polarization in response to incident

electromagnetic waves, while the imaginary component (ϵ_i) indicates the absorption of incident energy due to dipole motion.⁴² The dielectric constants can be calculated from Eqs. (7)–(9),

$$\epsilon = \epsilon_r + i\epsilon_i, \quad (7)$$

where

$$\epsilon_r = \eta^2 - K^2 \quad (8)$$

and

$$\epsilon = 2\eta K. \quad (9)$$

Figure 10 shows ϵ_r and ϵ_i components of $\text{Cu}_2\text{ZnSnS}_4$ and $\text{Li}_x\text{Cu}_{2-x}\text{ZnSnS}_4$ thin films as a function of incident wavelength. It is obvious that the variation of ϵ_r is mostly determined by η^2 due to small values of K^2 , but the variation of ϵ_i is primarily determined by K values, which are connected to the absorption coefficients. In the visible wavelength region, the real component of the dielectric function decreases with the increase in Li concentration, while the imaginary component increases after the addition of Li. This observation indicates that the energy absorption of the material from the electric field increases upon the incorporation of Li.

The optical conductivity was calculated using the following equation:⁴²

$$\sigma = \frac{\alpha n c}{4\pi}, \quad (10)$$

where σ , α , c , and n represent the optical conductivity, absorption coefficient, speed of light, and refractive index of the synthesized films, respectively.

Figure 11 shows the optical conductivity (OC) of all the synthesized samples. OC represents the enhancement of conductivity in the presence of photons. All the films exhibit remarkably high OC

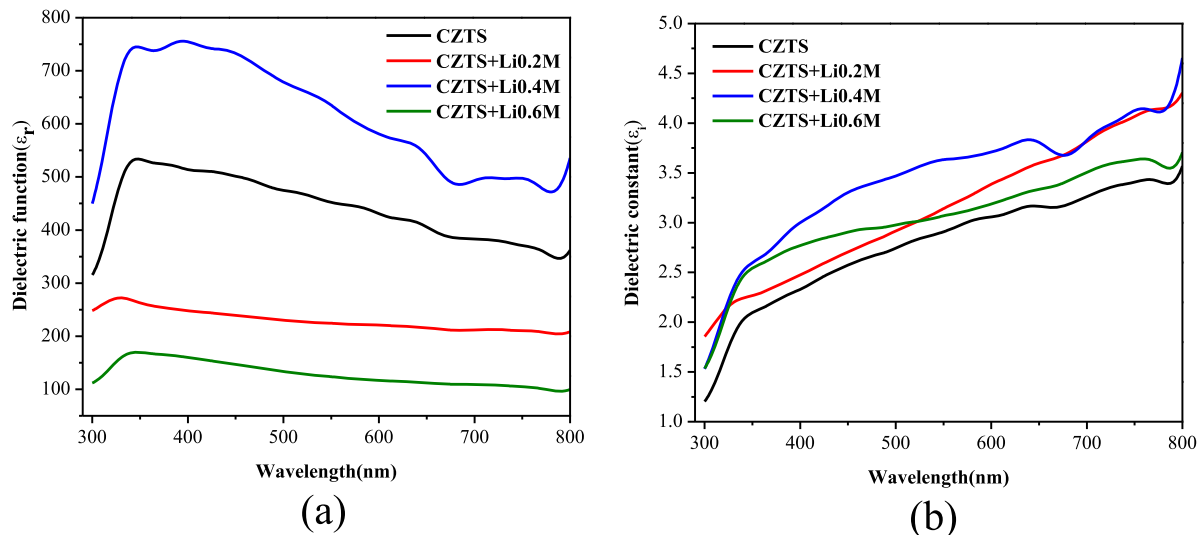


FIG. 10. (a) Real and (b) imaginary components of the dielectric constant of the prepared thin films.

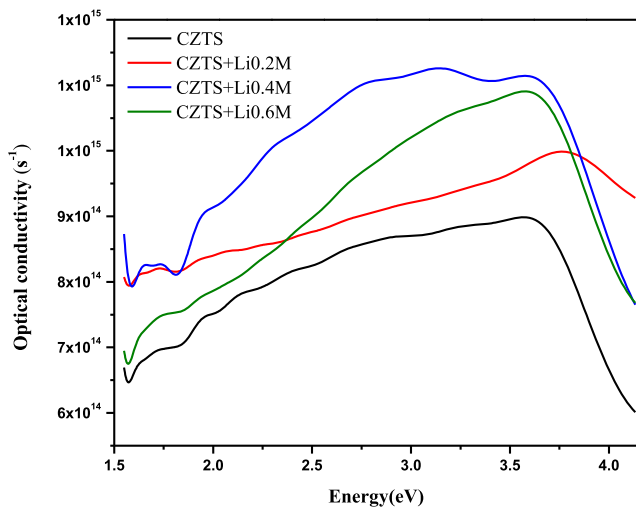


FIG. 11. Optical conductivity of the synthesized films.

values exceeding 10^{14} s^{-1} , making them suitable for various optoelectronic applications. The OC further increases with the rise in the Li content for the $\text{Li}_x\text{Cu}_{2-x}\text{ZnSnS}_4$ samples, indicating that Li atoms contribute to enhancing the optical response of CZTS thin films. Notably, all samples demonstrate heightened conductivity in the presence of blue wavelength compared to red wavelength, suggesting increased conductivity in response to high-energy photons.

IV. CONCLUSION

Thin films of both pristine and Li-doped CZTS were successfully synthesized through the spin coating technique. All films exhibited a tetragonal crystalline structure in the kesterite phase, characterized by reduced dislocations and stacking faults with increasing Li content. The incorporation of Li led to an improved periodicity in the CZTS structure. In addition, a fine film coverage was observed, accompanied by a reduction in average grain size attributed to the presence of Li. Li doping also showed improved optical properties with a high absorption coefficient and conductivity of 10^4 cm^{-1} and 10^{15} s^{-1} order, respectively, which can provide better performance as solar cell absorber layer material. The incorporation of Li content slightly increased the bandgap from 1.5 to 1.808 eV. The optimal bandgap within the visible energy range, coupled with a higher absorption coefficient and optical conductivity, suggests that Li-doped CZTS holds potential not only for solar cell absorber layers but also for various other optoelectronic applications.

ACKNOWLEDGMENTS

This research was supported by the Condensed Matter Physics lab at Jahangirnagar University in Dhaka, Bangladesh. We are grateful for financial support from the Ministry of Science and Technology, Bangladesh.

This study was funded by NST Fellowship 2021–2022 under the Ministry of Science and Technology, Bangladesh.

AUTHOR DECLARATIONS

Conflict of Interest

The authors declare that they have no conflict of interest.

Author Contributions

Md. Maruf Chand: Data curation (equal); Formal analysis (equal); Methodology (equal); Visualization (equal); Writing – original draft (equal). **Shariful Islam:** Project administration (equal); Software (equal); Validation (equal); Writing – review & editing (equal). **Mohammad Tanvir Ahmed:** Formal analysis (equal); Investigation (equal); Validation (equal); Writing – review & editing (equal). **Muhammad Shahriar Bashar:** Data curation (equal); Resources (equal). **Farid Ahmed:** Project administration (lead); Software (equal); Supervision (lead); Validation (equal).

DATA AVAILABILITY

The data that support the findings of this study are available from the corresponding author upon reasonable request.

REFERENCES

- M. P. Suryawanshi, G. L. Agawane, S. M. Bhosale, S. W. Shin, P. S. Patil, J. H. Kim, and A. V. Moholkar, *Mater. Technol.* **28**, 98 (2013).
- M. T. Ahmed, S. Hasan, S. Islam, and F. Ahmed, *Appl. Surf. Sci.* **623**, 157083 (2023).
- S. Kartik, D. Prakash, R. R. Kumar, V. Ramkumar, K. Vishista, H. S. Rathore, R. C. Panda, and T. Senthilvelan, *Polym. Bull.* **78**, 3527 (2021).
- Y. Anil Kumar, G. Koyyada, T. Ramachandran, J. H. Kim, S. Sajid, M. Moniruzzaman, S. Alzahmi, and I. M. Obaidat, *Nanomaterials* **13**, 1049 (2023).
- T. Ramachandran, A. H. I. Mourad, and F. Hamed, *Energies* **15**(10), 3754 (2022).
- D. Barik, M. Arun, M. A. Saeed, and T. Ramachandran, *Energies* **16**(1), 295 (2023).
- P. Jackson, D. Hariskos, R. Wuerz, O. Kiowski, A. Bauer, T. M. Friedlmeier, and M. Powalla, *Phys. Status Solidi RRL* **9**, 28 (2015).
- A. Soni, V. Gupta, C. M. Arora, A. Dashora, and B. L. Ahuja, *Sol. Energy* **84**, 1481 (2010).
- S. K. Swami, A. Kumar, and V. Dutta, *Energy Procedia* **33**, 198 (2013).
- J. Wang, Y. Wang, H. Li, A. Zhao, B. Li, J. Bi, and W. Li, *Mater. Sci. Semicond. Process.* **134**, 105943 (2021).
- J. Tao, J. Liu, J. He, K. Zhang, J. Jiang, L. Sun, P. Yang, and J. Chu, *RSC Adv.* **4**, 23977 (2014).
- E. Peksu and H. Karaagac, *J. Alloys Compd.* **862**, 158503 (2021).
- H. Katagiri, *Thin Solid Films* **480–481**, 426 (2005).
- K. Moriya, K. Tanaka, and H. Uchiki, “Fabrication of $\text{Cu}_2\text{ZnSnS}_4$ thin-film solar cell prepared by pulsed laser deposition,” *Jpn. J. Appl. Phys.* **46**, 5780 (2007).
- K. Pal, P. Singh, A. Bhaduri, and K. B. Thapa, *Sol. Energy Mater. Sol. Cells* **196**, 138 (2019).
- S. Dridi, G. El Fidha, N. Bitri, F. Chaabouni, and I. Ly, *Indian J. Phys.* **94**, 1097 (2020).
- S. Azmi, A. Moujib, O. A. Layachi, E. Matei, A. C. Galca, M. Y. Zaki, M. Secu, M. I. Rusu, C. E. A. Grigorescu, and E. M. Khomri, *J. Alloys Compd.* **842**, 155821 (2020).
- W. Li, J. M. R. Tan, S. W. Leow, S. Lie, S. Magdassi, and L. H. Wong, *Energy Technol.* **6**, 46 (2018).
- A. Ziti, B. Hartiti, H. Labrim, Y. Doubi, H. Joël Tchognia Nkuissi, Y. Nouria, S. Fadili, A. Batan, M. Tahri, A. Ridah, and P. Thevenin, *Mater. Today: Proc.* **53**, 355 (2022).
- T. Magorian Friedlmeier, N. Wieser, and T. Walter, “Heterojunctions based on $\text{Cu}_2\text{ZnSnS}_4$ and $\text{Cu}_2\text{ZnSnSe}_4$ thin films,” in European PVSEC, 1997.

- ²¹H. Wang, J. Li, and B. J. Kim, *Int. J. Photoenergy* **2011**, 801292 (2011).
- ²²H. Katagiri, K. Jimbo, S. Yamada, T. Kamimura, W. S. Maw, T. Fukano, T. Ito, and T. Motohiro, *Appl. Phys. Express* **1**, 041201 (2008).
- ²³T. K. Todorov, K. B. Reuter, and D. B. Mitzi, *Adv. Mater.* **22**, E156 (2010).
- ²⁴D. A. R. Barkhouse, O. Gunawan, T. Gokmen, T. K. Todorov, and D. B. Mitzi, *Prog. Photovoltaics: Res. Appl.* **20**, 6 (2012).
- ²⁵C. Yan, J. Huang, K. Sun, S. Johnston, Y. Zhang, H. Sun, A. Pu, M. He, F. Liu, K. Eder, L. Yang, J. M. Cairney, N. J. Ekins-Daukes, Z. Hameiri, J. A. Stride, S. Chen, M. A. Green, and X. Hao, *Nat. Energy* **3**, 764 (2018).
- ²⁶F. Liu, C. Yan, J. Huang, K. Sun, F. Zhou, J. A. Stride, M. Green, and X. Hao, *Adv. Energy Mater.* **6**, 1600046 (2016).
- ²⁷Z. Tong, C. Yan, Z. Su, F. Zeng, J. Yang, Y. Li, L. Jiang, Y. Lai, and F. Liu, *Appl. Phys. Lett.* **105**, 223903 (2014).
- ²⁸H. Xin, S. M. Vorpahl, A. D. Collord, I. L. Braly, A. R. Uhl, B. W. Krueger, D. S. Ginger, and H. W. Hillhouse, *Phys. Chem. Chem. Phys.* **17**, 23859 (2015).
- ²⁹X. F. Dong, T. T. Zheng, F. X. Yang, X. D. Sun, L. Yu, J. T. Chen, C. W. Wang, Y. Zhao, and Y. Li, *Sol. Energy Mater. Sol. Cells* **227**, 111102 (2021).
- ³⁰H. Guo, Y. Li, X. Guo, N. Yuan, and J. Ding, *Phys. B* **531**, 9 (2018).
- ³¹K. Muska, K. Timmo, M. Pilvet, R. Kaupmees, T. Raadik, V. Mikli, M. Grossberg-Kuusik, J. Krustok, R. Josepson, S. Lange, and M. Kauk-Kuusik, *Sol. Energy Mater. Sol. Cells* **252**, 112182 (2023).
- ³²Y. Yang, X. Kang, L. Huang, and D. Pan, *ACS Appl. Mater. Interfaces* **8**, 5308 (2016).
- ³³M. T. Ahmed, S. Islam, M. S. Bashar, M. A. Hossain, and F. Ahmed, *Adv. Mater. Sci. Eng.* **2022**, 7606339 (2022).
- ³⁴R. Tholkappiyan, R. Satheesh Kumar, L. Mohamed Azarudeen, G. Anand Kumar, K. Vishista, and F. Hamed, *Mater. Focus* **5**, 342 (2016).
- ³⁵R. K. Raji, V. Kurapati, T. Ramachandran, M. Muralidharan, R. Suriakarthick, M. Dhillip, and F. Hamed, *J. Mater. Sci. Mater. Electron.* **31**, 7998 (2020).
- ³⁶M. Arslan, A. Habib, M. Zakria, A. Mehmood, and G. Husnain, *J. Sci.: Adv. Mater. Devices* **2**, 79 (2017).
- ³⁷T. Ramachandran, S. Natarajan, and F. Hamed, *J. Electron Spectrosc. Relat. Phenom.* **242**, 146952 (2020).
- ³⁸M. T. Ahmed, S. Islam, M. S. Bashar, and F. Ahmed, *Cryst. Res. Technol.* **57**, 1 (2022).
- ³⁹A. Muiruri, M. Maringa, and W. du Preez, *Materials* **13**(23), 5355 (2020).
- ⁴⁰A. Q. Abdullah, *Chem. Mater. Res.* **3**, 10 (2013).
- ⁴¹R. K. Raji, T. Ramachandran, M. Muralidharan, R. Suriakarthick, M. Dhillip, A. Raja, V. Kurapati, F. Hamed, P. Ramasamy, and A. H. I. Mourad, *J. Mater. Sci. Mater. Electron.* **32**, 25528 (2021).
- ⁴²A. Ziti, B. Hartiti, H. Labrim, S. Fadili, H. J. Tchognia Nkuissi, A. Ridah, M. Tahri, and P. Thevenin, *Phys. Scr.* **97**, 065815 (2022).
- ⁴³M. T. Ahmed, S. Islam, and F. Ahmed, *Materialwiss. Werkstofftech.* **53**, 790 (2022).
- ⁴⁴S. Tombe, G. Adam, H. Heilbrunner, D. H. Apaydin, C. Ulbricht, N. S. Sari-ciftci, C. J. Arendse, E. Iwuoha, and M. C. Scharber, *J. Mater. Chem. C* **5**, 1714 (2017).
- ⁴⁵A. Lafond, C. Guillot-Deudon, J. Vidal, M. Paris, C. La, and S. Jobic, *Inorg. Chem.* **56**, 2712 (2017).